clade") within the large Eastern Eurasian cluster and are well separated from any other individuals, domestic or wild (D6 in Fig. 1). This evidence is consistent with a Lapita dispersal from Near to Remote Oceania, but the lack of any genetic affinity between this group and Taiwanese wild boar (Fig. 1) offers no support for the "Out-of-Taiwan" model (*23*) of human and pig dispersal into Near Oceania. This evidence also supports the importance of Halmahera, which has been shown to be the origin of Remote Oceanic populations of the Pacific rat (*Rattus exulans*) transported by Lapita peoples (*24*) and the origin of the human mitochondrial DNA (mtDNA) marker known as the "Polynesian motif" (*25*). The additional lack of affinity of the New Guinea pigs with *Sus celebensis* (the indigenous Sulawesi wild boar, also found on offshore islands including Halmahera) rules out a significant *S. celebensis* maternal genetic input as suggested by Groves (*16*).

The lack of an obvious genetic source population on either mainland or island Southeast Asia from which pigs in the Pacific clade were drawn is intriguing and may suggest either the existence of indigenous *S. scrofa* in Wallacea or an early human-mediated introduction from elsewhere in ISEA currently not sampled by our study. In either case, then ISEA must be considered another independent center of pig domestication. Interestingly, the two clades of *S. celebensis* (Fig. 1 and fig. S1) demonstrate that this group is not monophyletic. In fact, the North-South geographic partitioning of the two strongly implies two independent invasions of wild boar onto Sulawesi, a pattern identical to that reported for other Sulawesi fauna including macaques (*26*), shrews (*27*), and bovids (*28*). Lastly, an ISEA origin of the other sister taxa of *S. scrofa* (Javan warty pig, *S. verrucosus*, and the bearded pig, *S. barbatus*) is supported by the phylogenetic tree, although the paraphyletic arrangement provides no support for current species designations. Thus, further studies using both mtDNA and nuclear DNA are required to resolve the phylogenetic status of these taxa.

The genetic evidence presented in this study provides clear proof for multiple centers of domestication across Eurasia. To further examine the domestication of pigs, the zooarcheological records of Europe, India, Southeast Asia, and ISEA should be explored in more detail.

References and Notes

1. N. Benecke, in *Exploitation des Animaux Sauvages à travers le Temps*, J. Desse, F. Audoin-Rouzeau, Eds. (Editions APDCA, Juan-les-Pins, 1993), pp. 233–245.
2. J. Epstein, M. Bichard, in *Evolution of Domesticated Animals*, I. L. Mason, Ed. (Longman, New York, 1984), pp. 145–162.
3. E. Giuffra *et al.*, *Genetics* **154**, 1785 (2000).
4. Y. Jing, R. K. Flad, *Antiquity* **76**, 724 (2002).
5. J. Peters, D. Helmer, A. von den Driesch, M. Saña Seguí, *Paléorient* **25**, 27 (1999).
6. A. Ervynck, K. Dobney, H. Hongo, R. Meadow, *Paléorient* **27**, 47 (2002).
7. S. Bökönyi, *History of Domestic Mammals in Central and Eastern Europe* (Akademiai Kiado, Budapest, 1974).
8. C. S. Troy *et al.*, *Nature* **410**, 1088 (2001).
9. P. Rowley-Conwy, in *The Widening Harvest*, A. Ammerman, P. Biagi, Eds. (Archaeological Institute of America, Boston, 2003), pp. 99–117.
10. T. Jansen *et al.*, *Proc. Natl. Acad. Sci. U.S.A.* **99**, 10905 (2002).
11. P. Savolainen, Y. P. Zhang, J. Luo, J. Lundeberg, T. Leitner, *Science* **298**, 1610 (2002).
12. J. M. H. Kijas, L. Andersson, *J. Mol. Evol.* **52**, 302 (2001).
13. Materials and methods are available as supporting material on *Science* Online.
14. F. Ronquist, J. P. Huelsenbeck, *Bioinformatics* **19**, 1572 (2003).
15. H. J. Bandelt, P. Forster, A. Rohl, *Mol. Biol. Evol.* **16**, 37 (1999).
16. C. P. Groves, *Ancestors for the Pigs: Taxonomy and Phylogeny of the Genus* Sus (Tech. Bull. 3, Department of Prehistory, Research School of Pacific Studies, Australian National Univ., Canberra, 1981), 96 pp.
17. P. M. Heise-Pavlov, S. R. Heise-Pavlov, *Wildl. Biol.* **9**, 21 (2003).
18. J. D. Vigne, *Les mammiféres post-glaciaires de Corse: Etude archéozoologique* (Gallia préhistoire, suppl. 26, Editions du CNRS, Paris, 1988).
19. M. Apollonio, E. Randi, S. Toso, *Boll. Zool.* **3**, 213 (1988).
20. P. V. Kirch, *On the Road of the Winds: An Archaeological History of the Pacific Islands before European Contact* (Univ. of California Press, Berkeley, CA, 2000), 424 pp.
21. S. Bulmer, *J. Soc. Océan.* **31**, 7 (1975).
22. J. Golson, P. J. Hughes, *J. Soc. Océan.* **36**, 294 (1976).
23. M. E. Hurles, E. Matisoo-Smith, R. D. Gray, D. Penny, *Trends Ecol. Evol.* **18**, 531 (2003).
24. E. Matisoo-Smith, J. H. Robins, *Proc. Natl. Acad. Sci. U.S.A.* **101**, 9167 (2004).
25. S. J. Oppenheimer, M. B. Richards, *Nature* **410**, 166 (2001).
26. B. J. Evans, J. C. Morales, J. Supriatna, D. J. Melnick, *Biol. J. Linn. Soc.* **66**, 539 (1999).
27. M. Ruedi, *Biol. J. Linn. Soc.* **58**, 197 (1996).
28. H. Kako, T. Namikawa, O. Takenaka, A. Takenaka, T. Amano, H. Martojo, *Z. Zool. Syst. Evol.* **32**, 1 (1994).

29. We thank the Wellcome and Leverhulme Trusts, the Arts and Humanities Research Board, and the European Union PigBioDiv2 project for financial support. We are especially grateful to the Smithsonian Institution Museum of Natural History and to the many other institutions and individuals listed in the SOM that provided sample material and access to collections.

Supporting Online Material

www.sciencemag.org/cgi/content/full/307/5715/1618/DC1
Materials and Methods
Figs. S1 to S4
Tables S1 to S4
References and Notes

29 October 2004; accepted 18 January 2005
10.1126/science.1106927

High-Throughput Mapping of a Dynamic Signaling Network in Mammalian Cells

Miriam Barrios-Rodiles,[1] Kevin R. Brown,[2] Barish Ozdamar,[1,3] Rohit Bose,[1,3] Zhong Liu,[1] Robert S. Donovan,[1] Fukiko Shinjo,[1] Yongmei Liu,[1] Joanna Dembowy,[1,3] Ian W. Taylor,[1,3] Valbona Luga,[1,3] Natasa Przulj,[4] Mark Robinson,[5] Harukazu Suzuki,[6] Yoshihide Hayashizaki,[6] Igor Jurisica,[2,4,7] Jeffrey L. Wrana[1,3]*

Signaling pathways transmit information through protein interaction networks that are dynamically regulated by complex extracellular cues. We developed LUMIER (for luminescence-based mammalian interactome mapping), an automated high-throughput technology, to map protein-protein interaction networks systematically in mammalian cells and applied it to the transforming growth factor–β (TGFβ) pathway. Analysis using self-organizing maps and *k*-means clustering identified links of the TGFβ pathway to the p21-activated kinase (PAK) network, to the polarity complex, and to Occludin, a structural component of tight junctions. We show that Occludin regulates TGFβ type I receptor localization for efficient TGFβ-dependent dissolution of tight junctions during epithelial-to-mesenchymal transitions.

Dynamic protein-protein interactions (PPIs) are key for cell signaling and dictate the timing and intensity of network outputs. Systematic mapping of PPI networks has thus far focused on static analyses in *Saccharomyces cerevisiae*, *Drosophila melanogaster*, and *Caenorhabditis elegans* (*1–5*). To begin building an understanding of how signaling networks convey information in vertebrates, we developed high-throughput LUMIER to systematically map PPIs in mammalian cells. This strategy uses *Renilla* luciferase enzyme (RL) fused to proteins of interest, which are then coexpressed with individual Flag-tagged partners in mammalian cells. Their interactions were determined by performing an RL enzymatic assay on immunoprecipitates using an antibody against Flag (Fig. 1A). As a model for a systematic study of cell signaling, we focused on the

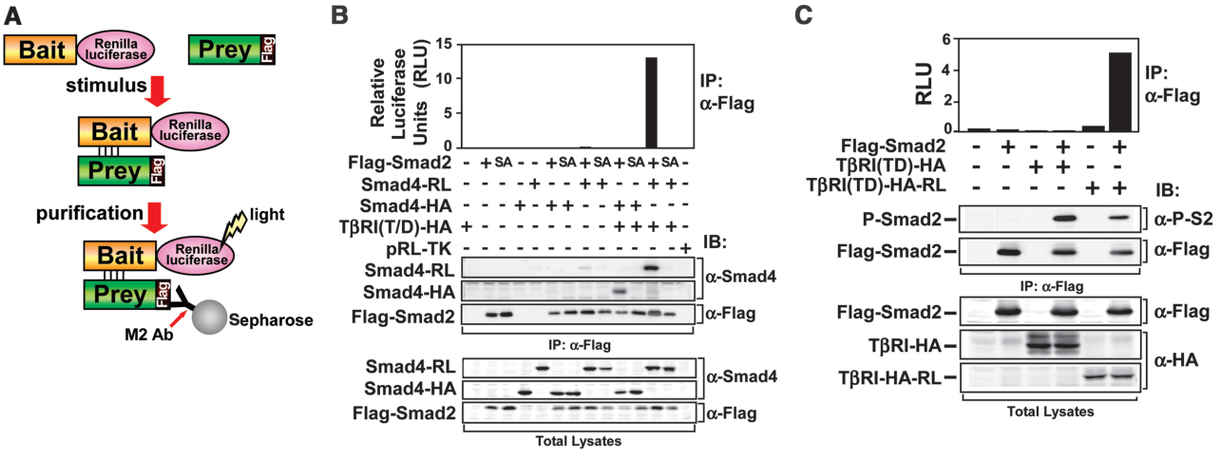

Fig. 1. A luminescence-based strategy for the detection of mammalian protein-protein interactions. (**A**) LUMIER. RL-tagged bait coexpressed with a Flag-tagged prey is detected in immunoprecipitates enzymatically as light emission. (**B**) LUMIER detects phosphorylation-dependent interactions. HEK-293T cells were transfected with hemagglutinin (HA)- or RL-tagged Smad4 together with either WT (+) or the phosphorylation site mutant (SA) of Flag-Smad2 in the absence (–) or presence (+) of TGFβ signaling. Smad4 interaction with Smad2 was determined by measuring RL activity on immunoprecipitates prepared using an antibody against Flag (histogram) or by immunoblotting (IB) with antibody against Smad4. pRL-TK is RL driven by the thymidine kinase promoter and is a negative control. (**C**) Detection of TβRI-Smad2 interaction by LUMIER. HEK-293T cells were transfected with constitutively active TβRI(T204D)-HA-RL or TβRI(T204D)-HA mutants in which Thr^{204} was replaced by Asp along with Flag-Smad2, and their association was detected as in (B, top panel). Levels of phosphorylated Smad2, total Smad2, and receptors were confirmed by immunoblotting with antibodies against phospho-Smad2 (α-P-S2), Flag, and HA, respectively (lower panels). Note that the TβRI(T204D)-Smad2 association cannot be detected by immunoblotting as it is a transient interaction.

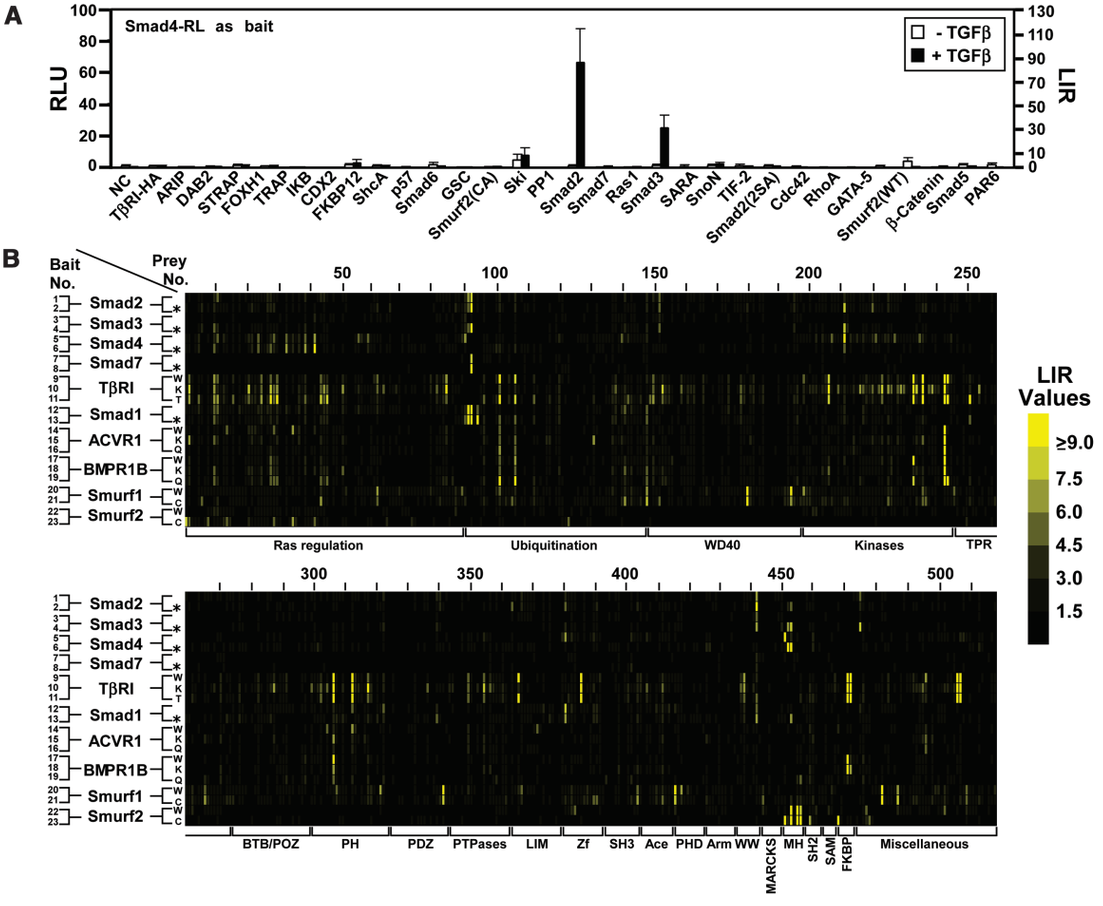

Fig. 2. High-throughput LUMIER. (**A**) Pilot screen in 96-well plates. HEK-293T cells were transfected with Smad4-RL and either empty vector (NC), HA-tagged TβRI (TβRI-HA), or 30 different Flag-tagged cDNAs (indicated) in the absence (white) or presence (black) of TGFβ signaling. Their interactions were assessed by LUMIER on immunoprecipitates prepared using an antibody against Flag. Results are plotted as the mean relative luciferase activity (RLU) ± SD of triplicates with corresponding luminescence intensity ratio (LIR) values shown on the right vertical axis. (**B**) The TGFβ pathway LUMIER screen. TGFβ pathway components (listed on the left) fused to RL were screened against 518 3Flag-tagged preys (numbered at the top of the panels and grouped by domain composition as indicated on the bottom) in the presence (*) or absence of TGFβ signal. Each row corresponds to the indicated pathway component and the LIR score for each test is represented in yellow, with the intensity representing the LIR value according to the scale on the right. W, wild type; K, kinase deficient; Q and T, constitutively active; and C, catalytically inactive.

TGFβ superfamily of extracellular morphogens, which regulates a plethora of biological processes in metazoans (*6*, *7*). TGFβs signal through ligand-induced heteromeric receptor complexes of type II and type I transmembrane serine-threonine kinases, which are activated when the type II receptor kinase transphosphorylates the type I receptor (fig. S1A). This stimulates binding and phosphorylation of receptor-regulated Smads (R-Smads) by the type I receptor. Phosphorylated R-Smads then dissociate from the receptor and form a complex with Smad4, and this complex then accumulates in the nucleus where it regulates transcription by interacting with DNA binding proteins (*7*, *8*).

The Smad pathway provides an example of how posttranslational modifications (PTMs) regulate the dynamics of PPI networks to control signal transduction (*9*). Therefore, we used this pathway to determine whether LUMIER could map PTM-dependent interactions. For this, we fused RL to Smad4 (Smad4-RL) and coexpressed it with Flag-Smad2 or the TGFβ receptor phosphorylation site mutant, Flag-Smad2(2SA), which does not bind Smad4. In the absence of signaling, little if any Smad4-RL was found associated with Smad2 (Fig. 1B), whereas TGFβ signaling induced a strong association with wild-type (WT) Smad2 that was revealed by high levels of RL activity in the immune complexes (*10*). In contrast, no Smad4-RL was detected in Smad2(2SA) immunoprecipitates. Similar results were obtained when we switched the tags for Smad2 and Smad4 (*11*). LUMIER also detected signal-specific interactions in the TGFβ-related bone morphogenetic protein (BMP) pathway (fig. S1B), constitutive interactions such as that between Smad4 and SnoN (fig. S1C), and transient substrate-enzyme interactions between Smad2 and active TGFβ type I receptor (TβRI) (Fig. 1C), which are difficult to detect by traditional means. Next, we optimized LUMIER in a 96-well format and performed a pilot-screen of Smad4-RL against 30 different Flag-tagged cDNAs in the presence or absence of TGFβ signaling (Fig. 2A). This revealed low background and strong, signal-dependent interactions between Smad4-RL and either Flag-Smad2 or Flag-Smad3, as well as the signal-independent interaction of Smad4-RL with Flag-Ski (*12*).

To map a TGFβ PPI network, we RL-tagged core members of the pathway (table S1) and 3×Flag-tagged (3Flag) 518 cDNAs from the FANTOM1 library (*13*) (fig. S2). These cDNAs encode proteins that contain at least one of the domains summarized in Fig. 2B (*10*). Each tagged protein was transiently expressed in mammalian cells, and their expression and subcellular localization were characterized (fig. S3) (*10*, *14*). To analyze the interaction of each RL-tagged TGFβ pathway component in different signaling contexts (table S1) with every Flag-tagged protein required about 12,000 experiments. Therefore, we used a robotics platform and performed automated LUMIER (*10*). To visualize the entire dataset, we generated a diagram in which each screen with RL-tagged protein is represented on the vertical axis and Flag-tagged proteins are on the horizontal axis (Fig. 2B). The results of each PPI test are represented by a bar at the intersection, with the intensity of yellow color reflecting that of the interaction, calculated as fold change over the negative control (*10*). We refer to this as the LUMIER intensity ratio (LIR) (see table S2 for all LIR values).

At low LIRs, background noise predominates, resulting in high false-positive rates and a noisy network, whereas at higher LIRs, interactions will be of higher confidence, but interactions that may be transient, occur in specific compartments, or are of lower affinity will be lost. Therefore, to build the interaction network graph, we examined false-negative rates and false-positive rates (*10*) and chose a conservative LIR cutoff of 3. This yielded false-negative rates of 36% (table S3) and false-positive rates of ~20%. The TGFβ interaction network at this cutoff revealed 947 interactions from 11,914 tests (table S2) that formed an interconnected network with nodes displaying degrees that ranged from 1 to 134 (table S4). The network

[1]Program in Molecular Biology and Cancer, Samuel Lunenfeld Research Institute, Mount Sinai Hospital, Toronto, Ontario, Canada, M5G 1X5. [2]Department of Medical Biophysics, University of Toronto, Toronto, Ontario, Canada, M5G 2M9. [3]Department of Medical Genetics and Microbiology, University of Toronto, Toronto, Ontario, Canada, M5S 1A8. [4]Department of Computer Science, University of Toronto, Toronto, Ontario, Canada, M5S 3H5. [5]Banting and Best Department of Medical Research, University of Toronto, Toronto, Ontario, Canada, M5G 1L6. [6]Laboratory for Genome Exploration Research Group, RIKEN Genomic Sciences Center (GSC), Yokohama Institute, 1-7-22 Suehiro-cho, Tsurumi-ku, Yokohama, 230-0045, Japan. [7]Division of Cancer Informatics, Ontario Cancer Institute, Princess Margaret Hospital, Toronto, Ontario, Canada, M5G 2M9.

*To whom correspondence should be addressed. E-mail: wrana@mshri.on.ca

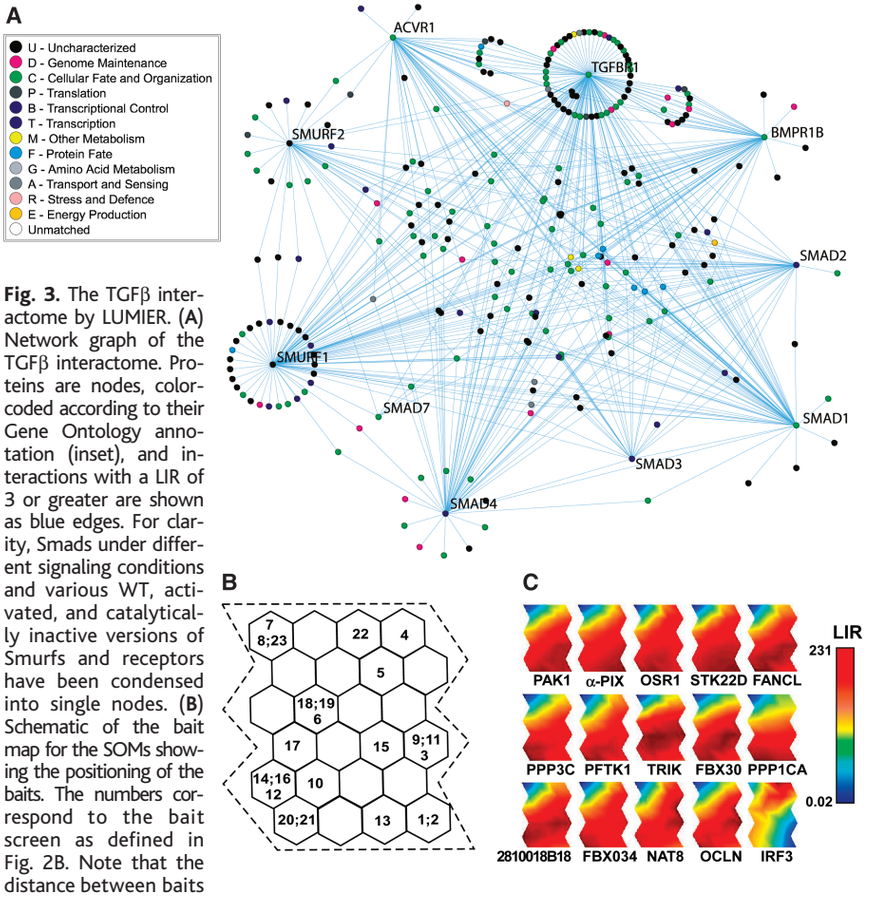

Fig. 3. The TGFβ interactome by LUMIER. (**A**) Network graph of the TGFβ interactome. Proteins are nodes, color-coded according to their Gene Ontology annotation (inset), and interactions with a LIR of 3 or greater are shown as blue edges. For clarity, Smads under different signaling conditions and various WT, activated, and catalytically inactive versions of Smurfs and receptors have been condensed into single nodes. (**B**) Schematic of the bait map for the SOMs showing the positioning of the baits. The numbers correspond to the bait screen as defined in Fig. 2B. Note that the distance between baits reflects the similarity in their interaction profile with the 518 preys. Thus, baits that behave similarly are close to each other and when very similar can occupy the same position. (**C**) Combined unsupervised and supervised BTSVQ clustering of the LUMIER data identifies a group of proteins with similar SOMs. IRF3 (lower right), which is part of a different cluster, is shown for comparison.

displayed features of a scale-free network with possible hierarchical modularity (*10*) (fig. S4), which have also been noted in other PPI networks (*15*). Network dynamics are important in understanding signaling networks (*16*), which must be remodeled in time and space to convey information. To determine how signaling regulates PPIs in our network, we focused on the dynamics of the Smad2 and Smad4 interactome in the absence and presence of TGFβ signaling (fig. S5). To capture the dynamics, we also generated a movie of the network changes (movie S1). Analysis of these graphs and the movie revealed considerable partner switching; numerous interactions were lost upon signaling, whereas others, such as the assembly of Smad complexes, were stimulated.

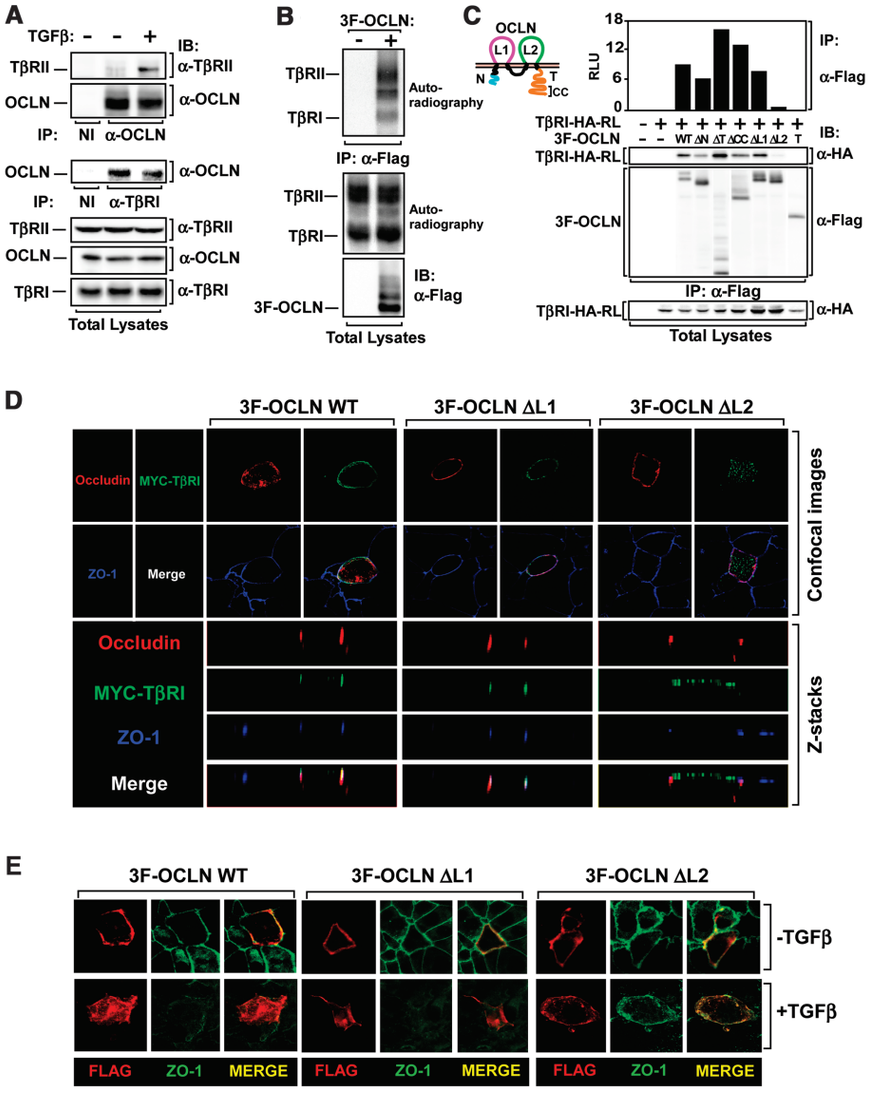

Fig. 4. OCLN regulates TGFβ-dependent dissolution of tight junctions. Interaction between endogenous OCLN and type I and type II receptors in untreated (–) or TGFβ-stimulated (+) NMuMG cells (**A**) or with affinity-labeled TGFβ receptors expressed on HEK-293T cells (**B**) was analyzed as described (*10*). (**C**) Mapping the TβRI interaction domain on OCLN using LUMIER. WT TβRI-HA-RL was expressed alone or together with WT or mutant OCLN harboring the indicated domain deletions (see schematic), and interactions were measured by LUMIER (top panel) or by immunoblotting with antibody against HA. Expression of proteins was confirmed by immunoblotting total cell lysates, as indicated. (**D**) Localization of OCLN, OCLN(ΔL1), OCLN(ΔL2), and cell surface TβRI in polarized NMuMG epithelial cells. WT 3Flag-tagged OCLN or the indicated mutants (red) were expressed together with Myc-tagged TβRI (green), and protein subcellular localization in tight junctions (ZO-1, blue) was visualized as described (*10*). The overlay shows colocalization of all three proteins as white (MERGE). (**E**) OCLN(ΔL2) inhibits TGFβ-induced EMT. NMuMG cells transiently expressing the indicated WT or OCLN mutants were untreated (–) or treated (+) with TGFβ for 24 hours. OCLN-expressing cells were identified by staining with antibody against Flag, and tight junctions were visualized by staining with antibodies against ZO-1. Confocal optical slices of the tight junction region are shown.

LUMIER can thus detect in mammalian cells pathway-specific, PTM-dependent PPIs, constitutive protein interactions, and interactions involving transmembrane receptors. The last mentioned is noteworthy, as transmembrane receptors are critical focal points in signaling networks, are important drug targets, and have been difficult to study with other high-throughput approaches (*17*). However, we have not yet been able to measure the concentration of the Flag-tagged preys in high-throughput LUMIER; therefore, we cannot measure absolute PPI affinities. Furthermore, overexpression can be useful for detecting interactions that occur between proteins of low abundance, as well as weak or transient interactions, but this can also make the assay prone to false positives. These advantages and disadvantages should be taken into account when evaluating LUMIER networks.

To identify novel TGFβ signaling networks of biological importance, we explored the TGFβ LUMIER dataset using the binary tree–structured vector quantization (BTSVQ) algorithm (*10*, *18*). BTSVQ performs unsupervised clustering and supports intuitive visualization of the data, both as a binary tree dendrogram and as Kohonen's self-organizing maps (SOMs), providing a powerful method for visualizing complex datasets that effectively exploits the semiquantitative information inherent in LUMIER. To identify novel targets of the TGFβ pathway, we focused on clustering the Flag-tagged proteins (preys). For this, the algorithm first analyzed the interaction of each RL-tagged bait with the library of Flag-tagged preys and organized the placement of baits according to their interaction profiles with all of the preys (see Fig. 3B for map of bait positions). Therefore, baits that display different interaction profiles are far apart, whereas baits displaying similar profiles are close (Fig. 3B). When bait profiles are very similar they can occupy the same map unit position. Once the positions of the baits are fixed, a SOM is generated for each prey, in which the interaction of that prey with each of the baits is projected onto the bait map, with the color representing the LIR value. Unlabeled map units are interpolated to make the color homogeneous (Fig. 3C).

BTSVQ analysis thus identified clusters of prey proteins that displayed similar patterns of interactions with the TGFβ pathway (that is, similar SOM patterns). One of these clusters included PAK1, a member of the PAK family, which is involved in regulating cytoskeletal dynamics, cell motility, survival, proliferation, and gene expression through a variety of effectors (*19*) and has been implicated in TGFβ signaling (*20*). However,

physical association with TGFβ pathway components has not been reported. Therefore, we anchored our unsupervised clustering on PAK1 and sorted prey SOMs to identify similar profiles. The resulting cluster (Fig. 3C) contained known PAK1-binding proteins, such as the PAK-interacting Cdc42 exchange factor, ARHGEF6 (α-PIX), and oxidative stress–response kinase-1 (OSR1) (*19*, *21*), as well as Occludin (OCLN), a tight junction accessory protein that is associated with the cell polarity network (*22*) (fig. S7A). Therefore, we validated the interaction of a number of these proteins with TGFβ receptors (fig. S6) (*10*), which included validating interactions between endogenous TβRI and both PAK1 and OCLN. Further, although physical links reported between PAK1 and Polarity-OCLN networks are few (fig. S7A), analysis of LUMIER data revealed substantial connections between the TGFβ pathway and both networks (fig. S7B).

TGFβ induces dissolution of tight junctions and acquisition of a mesenchymal phenotype in breast epithelial culture models (*23*, *24*). Therefore, we examined the OCLN-TGFβ receptor complex in normal mammary gland epithelial cells (NMuMG). Interaction of endogenous OCLN with endogenous TβRI was not modulated by TGFβ (Fig. 4A), whereas its association with the TGFβ type II receptor increased in a ligand-dependent manner (Fig. 4A) and OCLN interacted with cell surface affinity–labeled TGFβ receptor complexes (Fig. 4B). Using LUMIER, we mapped the TβRI-interacting region of OCLN to extracellular loop 2 (L2) (Fig. 4C). TβRI is localized to tight junctions in polarized NMuMG cells (*25*). To determine whether OCLN might contribute to regulating TβRI localization, we used OCLN(ΔL2) as a dominant negative. Confocal microscopy in polarized NMuMG cells revealed that the WT, as well as the extracellular loop 1 (ΔL1) and ΔL2 mutants of OCLN, localized with ZO-1 on the apical aspect of the cell in tight junctions (Fig. 4D). Localization of Myc-tagged TβRI in tight junctions was unaffected by WT OCLN or OCLN(ΔL1), both of which interacted with TβRI. In contrast, OCLN(ΔL2) caused mislocalization of TβRI across the surface of the cell (Fig. 4D). Moreover, when we examined the epithelial-to-mesenchymal transition (EMT) in these cells, 40% of OCLN(ΔL2)-expressing cells exhibited retained tight junctions after TGFβ treatment, compared with only 10% of control cells (Fig. 4E) (*11*). In contrast, none of the OCLN mutants affected TGFβ-dependent induction of a Smad-responsive reporter gene (fig. S8). Thus, OCLN regulates TβRI localization to tight junctions, and this is important for efficient TGFβ-dependent dissolution of tight junctions during EMT. This suggests that targets of the receptor complex localized to tight junctions are involved in EMT, and in a separate study, we show that Par6, a key regulatory component of tight junctions, is an important downstream effector of this pathway (*25*). Our results provide a systematic analysis in mammalian cells of protein interactions involved in cell signaling and highlight how these approaches can uncover new connectivities in mammalian signaling pathways.

References and Notes

1. P. Uetz *et al.*, *Nature* **403**, 623 (2000).
2. A. C. Gavin *et al.*, *Nature* **415**, 141 (2002).
3. Y. Ho *et al.*, *Nature* **415**, 180 (2002).
4. L. Giot *et al.*, *Science* **302**, 1727 (2003).
5. S. Li *et al.*, *Science* **303**, 540 (2004).
6. A. B. Roberts, L. M. Wakefield, *Proc. Natl. Acad. Sci. U.S.A.* **100**, 8621 (2003).
7. R. Derynck, Y. E. Zhang, *Nature* **425**, 577 (2003).
8. L. Attisano, J. L. Wrana, *Science* **296**, 1646 (2002).
9. T. Pawson, *Cell* **116**, 191 (2004).
10. Materials and methods are available as supporting material on *Science* Online.
11. M. Barrios-Rodiles, B. Ozdamar, unpublished data.
12. K. Luo *et al.*, *Genes Dev.* **13**, 2196 (1999).
13. J. Kawai *et al.*, *Nature* **409**, 685 (2001).
14. All subcellular localization data and LUMIER results can be found at http://ophid.utoronto.ca/LUMIER/.
15. S. H. Yook, Z. N. Oltvai, A. L. Barabasi, *Proteomics* **4**, 928 (2004).
16. J.-D. J. Han *et al.*, *Nature* **430**, 88 (2004).
17. I. Stagljar, S. Fields, *Trends Biochem. Sci.* **27**, 559 (2002).
18. M. Sultan *et al.*, *Bioinformatics* **18** (suppl. 1), S111 (2002).
19. G. M. Bokoch, *Annu. Rev. Biochem.* **72**, 743 (2003).
20. M. C. Wilkes, S. J. Murphy, N. Garamszegi, E. B. Leof, *Mol. Cell. Biol.* **23**, 8878 (2003).
21. W. Chen, M. Yazicioglu, M. H. Cobb, *J. Biol. Chem.* **279**, 11129 (2004).
22. L. Gonzalez-Mariscal, A. Betanzos, P. Nava, B. E. Jaramillo, *Prog. Biophys. Mol. Biol.* **81**, 1 (2003).
23. S. E. Seton-Rogers *et al.*, *Proc. Natl. Acad. Sci. U.S.A.* **101**, 1257 (2004).
24. M. Oft *et al.*, *Genes Dev.* **10**, 2462 (1996).
25. B. Ozdamar *et al.*, in press.

26. We thank L. Attisano for critical review and support throughout this project and members of the Attisano and Wrana labs for cDNA reagents, advice, and encouragement throughout this project, especially C. Le Roy, S. Bonni, L. Izzi, and E. Labbé for the Smad subnetwork movie. Work in J.L.W.'s lab was supported by funds from Genome Canada, the Natural Sciences and Engineering Research Council (NSERC), the Canadian Institutes of Health Research (CIHR), and the National Cancer Institute of Canada with funds from the Canadian Cancer Society. Work in I.J.'s lab is supported by NIH (P50 GM-62413), NSERC, an International Business Machines (IBM) Shared University Research and IBM Faculty partnership, and from the Institute for Robotics and Intelligent Systems (IRIS). The RIKEN Genomic Sciences Center is supported by the Genome Network Project and the Advanced and Innovational Research Program in Life Science, both from the Ministry of Education, Culture, Sports, Science, and Technology, as well as the Core Research for Evolutional Science and Technology of the Japan Science and Technology Corp. M.B.-R. is a CIHR Postdoctoral Fellow; B.O. and R.B. hold Ph.D. and M.D./Ph.D. CIHR studentships, respectively; K.R.B. is supported by a scholarship from the Institute of Robotics and Intelligent Systems (Precarn Inc.); and N.P. holds an Ontario Graduate Scholarship. J.L.W. is an International Scholar of the Howard Hughes Medical Institute and a CIHR Senior Investigator.

Supporting Online Material

www.sciencemag.org/cgi/content/full/307/5715/1621/DC1
Materials and Methods
Figs. S1 to S8
Tables S1 to S4
Movie S1

28 September 2004; accepted 11 January 2005
10.1126/science.1105776

A Transmembrane Intracellular Estrogen Receptor Mediates Rapid Cell Signaling

Chetana M. Revankar,[1,2] Daniel F. Cimino,[1,2] Larry A. Sklar,[2,3] Jeffrey B. Arterburn,[4] Eric R. Prossnitz[1,2]*

The steroid hormone estrogen regulates many functionally unrelated processes in numerous tissues. Although it is traditionally thought to control transcriptional activation through the classical nuclear estrogen receptors, it also initiates many rapid nongenomic signaling events. We found that of all G protein–coupled receptors characterized to date, GPR30 is uniquely localized to the endoplasmic reticulum, where it specifically binds estrogen and fluorescent estrogen derivatives. Activating GPR30 by estrogen resulted in intracellular calcium mobilization and synthesis of phosphatidylinositol 3,4,5-trisphosphate in the nucleus. Thus, GPR30 represents an intracellular transmembrane estrogen receptor that may contribute to normal estrogen physiology as well as pathophysiology.

Estrogen (17β-estradiol, E2) represents one of a family of steroid hormones that act through soluble intracellular receptors. Once activated, these receptors translocate to the nucleus, where they function as ligand-dependent transcription factors (*1*, *2*). This mode of action of two such estrogen-binding receptors, ERα and ERβ, is reasonably well understood (*3*, *4*). However, the existence of functional ERs associated with the plasma membrane has been debated (*5*). It has been suggested that such membrane receptors me-